High Sensitivity Graphene Field Effect Transistor-Based Detection of DNA Amplification

Anurup Ganguli, Vahid Faramarzi, Ariana Mostafa, Michael T. Hwang, Seungyong You, and Rashid Bashir*

Enzymatic DNA amplification-based approaches involving intercalating DNA-binding fluorescent dyes and expensive optical detectors are the gold standard for nucleic acid detection. As components of a simplified and miniaturized system, conventional silicon-based ion sensitive field effect transistors (ISFETs) that measure a decrease in pH due to the generation of pyrophosphates during DNA amplification have been previously reported. In this article, Bst polymerase in a loop-mediated isothermal amplification (LAMP) reaction combined with target-specific primers and crumpled graphene field effect transistors (gFETs) to electrically detect amplification by sensing the reduction in primers is used. Graphene is known to adsorb single-stranded DNA due to noncovalent π–π bonds, but not double-stranded DNA. This approach does not require any surface functionalization and allows the detection of primer concentrations at the endpoint of reactions. As recently demonstrated, the crumpled gFET over the conventional flat gFET sensors due to their superior sensitivity is chosen. The endpoint of amplification reaction with starting concentrations down to 8×10^{-21} M in 90 min including the time of amplification and detection is detected. With its high sensitivity and small footprint, this platform will help bring complex lab-based diagnostic and genotyping amplification assays to the point-of-care.

1. Introduction

Rapid and accurate detection of infection causing pathogens such as *Escherichia coli* and others remains a challenge in healthcare.[1] State of the art for sensitive and specific detection of pathogens usually relies on their genomic DNA amplification using techniques such as polymerase chain reaction (PCR) or loop-mediated isothermal amplification (LAMP) which

require expensive optical readout instrumentation for measuring the fluorescence signal from intercalating DNA binding dyes.[2] Toward optics-free platforms, approaches using carbon nanotube and silicon nanowire field effect transistors for electrical and label-free DNA "hybridization-based" detection have been previously reported.[3,4,5,6] However, these DNA hybridization-based techniques often have a lower limit-of-detection (LOD) (pico-molar to femtomolar range),[6] as compared to the LOD of optics-based DNA amplification techniques (low attomolar range).[7,8] CMOS compatible ion sensitive field effect transistor (ISFET) arrays have also been used for hybridization-based DNA detection but with LOD usually in nanomolar range.[9] ISFETs have also been used for label-free electrical detection of DNA amplification by detecting pH changes during an amplification reaction.[10,11] However, these platforms often require special low buffer capacity reactions for detecting signals and have inferior performance (LOD > 10×10^{-18} M[10]) as compared to optical readout systems.

Toward electrical detection of biomolecules, graphene field-effect transistor-based biosensors (gFET) offer many potential advantages, such as large surface-to-volume ratio, high carrier mobility, and low cost.[12] Several gFET-based platforms offering high sensitivity, low cost, and high throughput detection using diverse sensing methods such as electrochemical,[13] back-gated gFETs,[14] and liquid-gated gFETs[15–18] have been reported in the literatures. The semiconductor–dielectric interface inside the conventional ISFET is not accessible for biomolecule functionalization and usually the analyte in the sample will be adsorbed/attached to the gate oxide and will modulate the capacitance and electric field across it.[16] In such devices, the gate oxide should be thin to better modulate the electric signal and increase the sensitivity of the device while also being thick enough to reduce the gate leakage current and increase signal-to-noise ratio.[19] In contrast, graphene electrolyte-gated FET biosensors can overcome these drawbacks as the transistor channel is formed by a single two-dimensional (2-D), one-atom-thick carbon layer, which can be left accessible for direct functionalization or adsorption with biomolecules. Hence, the local gating effect is much more effective than conventional devices.[20–26] Many studies have demonstrated the use of gFET sensor for biomolecules detection, including protein, DNA, and bacteria.[27]

Dr. A. Ganguli, A. Mostafa, Prof. R. Bashir
Department of Bioengineering
University of Illinois at Urbana-Champaign
Champaign, IL, USA
E-mail: rbashir@illinois.edu
Dr. A. Ganguli, V. Faramarzi, A. Mostafa, Dr. M. T. Hwang, Dr. S. You, Prof. R. Bashir
Nick Holonyak Jr. Micro and Nanotechnology Laboratory
University of Illinois at Urbana-Champaign
Champaign, IL, USA
Prof. R. Bashir
Carle Illinois College of Medicine
University of Illinois at Urbana-Champaign
Champaign, IL, USA

**ADVANCED
SCIENCE NEWS**

www.advancedsciencenews.com

**ADVANCED
FUNCTIONAL
MATERIALS**

www.afm-journal.de

To enable specific binding, gFETs can be functionalized with single-stranded probe DNA for detection of specific target DNA through DNA–DNA hybridization with complementary sequences. Using this DNA hybridization-based approach, gFETs typically offer a LOD ranging from 100×10^{-12} M to 1×10^{-15} M.[15,17,28–30] A further improvement of LOD, up to 25×10^{-18} M, was recently reported by optimizing the bio-FET channel and using a large-area in-plane gate surrounding the graphene channel that allows a uniform distribution of potential inside the water droplet and a uniform gating field.[19]

The net electrostatic effect of a charged molecule in the solution containing different ions is measured in terms of Debye length with characteristic thickness of less than 1 nm in physiological solutions.[19] Outside the Debye length, charge carriers are increasingly electrically screened. By increasing the Debye length, the sensitivity of the gFETs to detect target DNA can be enhanced because more sequence length of DNA strand is within the Debye length and thus more electric charge is induced near the graphene surface. This will result in a higher change in the electric conductance of the graphene channel. Previous computational studies have shown that curved morphologies, such as the concave regions of nanowire sensors, can affect the Debye length.[31] Studies have also reported that crumpled graphene, which has concave and convex deformations at the micro- and nanoscale can be fabricated using pre-strained thermoplastics and relieving stress to induce buckle delamination of graphene.[32] The mechanically tunable crumpled graphene has already been explored in several applications, such as stretchable photosensors[33] and strain gauges.[34] Its application in biosensing has also been recently reported with hybridization-based DNA detection with improved sensitivity.[35] The sensitivity enhancement in crumpled graphene in this recent study was attributed to the nanoscale deformations, specifically the concave regions, that decrease the charge screening of the nucleic acid molecules by increasing the Debye length in the ionic solution.[35] In addition, the crumpled graphene could form a bandgap in the deformed regions further allowing for an exponential source–drain current change from a small number of charges.[35] However, despite its improved sensitivity, this hybridization-based method still requires surface functionalization of the graphene channel and thus can lead to complications in fabrication process.

In this article, we show that crumpled gFETs can be used to detect physiosorbed single-stranded DNA (ssDNA) molecules (as compared to double-stranded DNA product) on its surface and use this for detecting enzymatic amplification by monitoring the reduction in primer (ssDNA) concentration in a reaction. Unlike double-stranded DNA (dsDNA), ssDNA can be strongly adsorbed on the gFET surface through noncovalent π–π stacking interaction between the hexagonal cells of graphene and the aromatic ring structure of unpaired nucleobases.[36–39] In our platform, we use this discrimination power of crumpled graphene coupled with primer (ssDNA) consumption in enzymatic LAMP[40] to detect *E. coli* DNA down to zeptomolar (zM) concentrations in endpoint LAMP reactions. gFET signal generated from primers is reduced only if the specific target is present and amplification occurs where primers are consumed during amplification and become a part of formed dsDNA. In contrast, the dsDNA produced in the amplification does not produce any significant shift in the Dirac voltage.

LAMP was chosen as our assay reaction as it uses a robust strand-displacement Bst polymerase and six sequence specific primers compared to the 2 used in PCR.[41] Moreover, since it is an isothermal reaction, the instrumentation demands are easier. LAMP is also known to be highly specific and sensitive and hence offers single molecule (attomolar) sensitivity for detecting target DNA.[42] We expect our platform, with its electrical, label-free and surface modification-free detection of enzymatic amplification, will allow translation of complex and sensitive lab-based amplification assays to truly point-of-care and small footprint detection devices.

2. Results and Discussion

2.1. Process Overview and Device Characterization for Physisorption of ssDNA and dsDNA

The approach for using crumpled gFET sensor for detection of LAMP reaction is illustrated in **Figure 1**. Amplification reagents, including target DNA-specific primers and Bst polymerase enzyme, are added to the target DNA (or negative control) in a reaction tube and isothermal DNA amplification is performed at 65 °C for 1 h. After 1 h, the complete reaction mix is diluted in 1X PBS and added to the crumpled gFET for 15 min to allow physisorption of molecules. After 15 min, the samples are rinsed in 1X PBS again and the Dirac point shifts due to the physiosorbed molecules are measured. Details on dilution and measurements can be found in the Materials and Methods section in Supporting Information. In the LAMP reaction, primer molecules which are ssDNA and present in excess in the reaction, bind to the target DNA and with the help of polymerase enzyme, copies of the target DNA are generated. In this process, the ssDNA primers are consumed and converted to dsDNA target copies.[43] Within 1 h, this results in consumption of primers and hence reduction of ssDNA concentration only in reactions where the specific target DNA was present. Since the formed dsDNA during amplification does not bind to crumpled graphene as strongly due to paired DNA bases which causes the π–π stacking sites to be inside the helix,[39] we see an overall lower Dirac voltage shift for samples containing the target DNA compared to negative control samples.

Our crumpled gFET biosensor fabrication process was adapted from previously published protocol.[32] Briefly, a 2×14 mm graphene channel was transferred onto a thermoplastic polystyrene substrate and annealed at 110 °C for 4 h. During the annealing process, the underlying pre-strained thermoplastic substrate shrinks and results in the buckling and crumpling of graphene channel. For the flat gFET used in this study, this annealing step was omitted. Finally, the source and drain metal electrodes are formed and an ionic solution reservoir was created around the graphene channel and gate voltage is applied directly to the top of the ionic solution placed in the reservoir in the device. The black regions in **Figure 2**a show the source and drain contacts, and graphene is visible as a shaded rectangular channel between source and drain contacts surrounded by solution reservoir. The morphology of the crumpled graphene surface shown by atomic force microscope (AFM) image in Figure 2b depicts disorganized structures with fine wrinkles as small as a few hundred nanometers. Theoretical
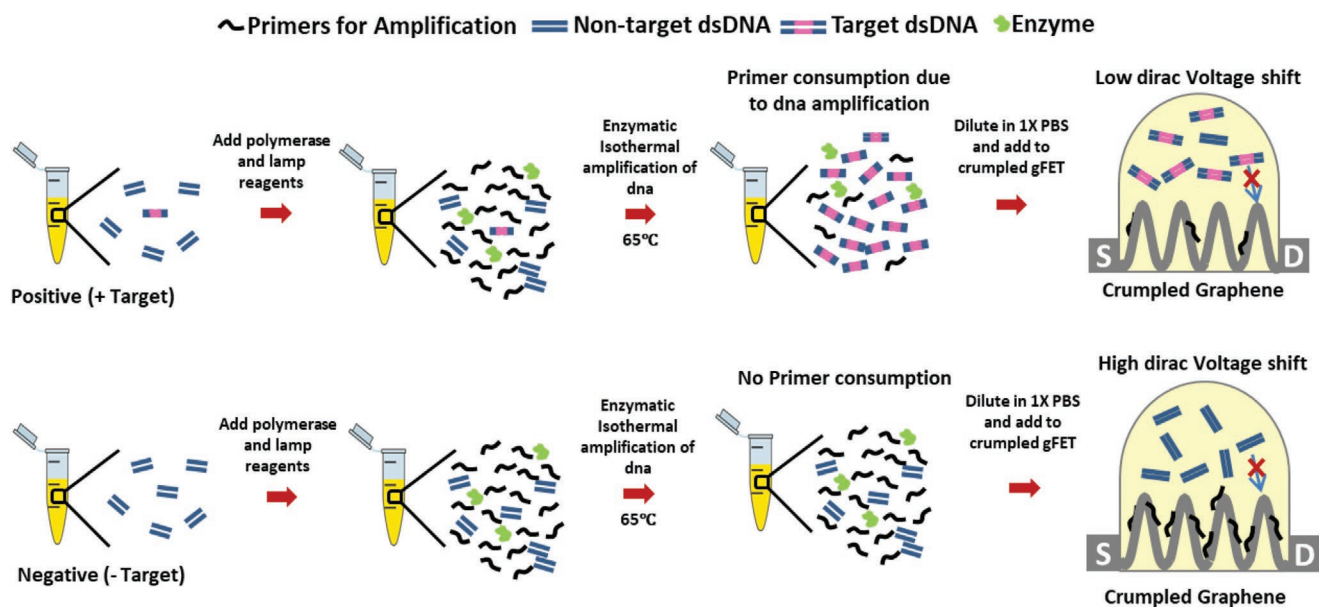
Figure 1. Approach for detecting enzymatic DNA amplification. Process overview of detecting target DNA using loop-mediated isothermal amplification (LAMP) followed by detection of primer (ssDNA) on gFET sensors. Schematic of crumpled gFET DNA sensor and its adsorption of ssDNA and not dsDNA. LAMP was used to amplify target DNA causing consumption and decrease of primer concentration. Reduced primer concentration post-amplification gives a lower Dirac voltage shift on the sensor.
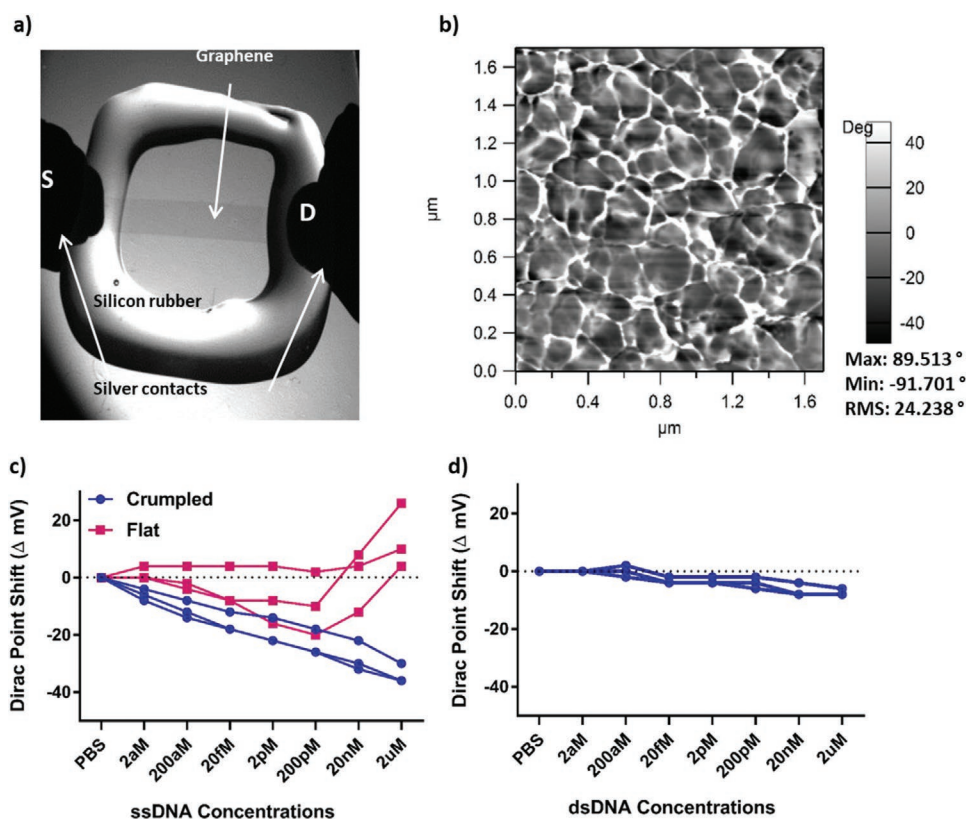

Figure 2. Characterization of the gFET and DNA adsorption studies. a) Microscopic optical image of the device. S and D indicate the source and drain contacts, respectively. Graphene channel is visible as shaded region in the middle. b) Phase image of the crumpled graphene clearly shows the nanoscale crumpling features on the graphene surface. Wrinkles as small as a few hundred nanometers can be seen. c) Dirac voltage shift of the FET sensor for ssDNA adsorption on flat and crumpled graphene ($n = 3$). d) Dirac voltage shift of the crumpled gFET sensor for dsDNA adsorption test. The Dirac point shift even for the highest concentrations of dsDNA (≈ 0 mV for 2×10^{-6} M dsDNA) is small in comparison to even very low concentrations of ssDNA (≈ 6 mV even for 2×10^{-18} M ssDNA) ($n = 3$).

**ADVANCED
SCIENCE NEWS**
www.advancedsciencenews.com

**ADVANCED
FUNCTIONAL
MATERIALS**
www.afm-journal.de

Debye length modulation in our crumpled gFET sensors can be expected to arise from these small concave wrinkles. The AFM topography data for crumpled graphene also shows increased surface roughness (RMS ≈17.49 nm) compared to flat graphene surface (RMS ≈0.65 nm) (Figure S5, Supporting Information). It is important to note that these estimated roughness values are often underestimated and are limited in resolution by AFM tip dimensions. To validate the electrical properties of crumpled graphene, source–drain current was measured and found to be between 4 and 8 kΩ.

Figure 2c shows the results of electrical sensing of ssDNA in 1X PBS for both flat and crumpled graphene. For the electrical sensing, changes in source–drain current and the Dirac voltage point shifts were measured due to physisorption of ssDNA molecules on our sensor. For ssDNA measurements, we chose FIP primer sequence (Supplementary Table 1), and tested the sequential increase in concentrations of ssDNA from 2×10^{-18} M to 2×10^{-6} M on the same device. More details about the measurement protocol is presented in the Materials and Methods section in Supporting Information. For flat graphene device, there was no significant Dirac point shift below 20×10^{-15} M, with an overall negative Dirac point shift of 10 mV from 2×10^{-18} M to 200×10^{-12} M. From 200×10^{-12} M to 2×10^{-6} M, anomalous positive Dirac point shifts of up to 26 mV were observed, possibly related to device stability issues as these tests were sequentially performed on the same device. We observed high device-to-device variability in flat graphene measurements resulting in larger error bars (std. dev. for $n = 3$) as compared to that of crumpled graphene measurements. For crumpled graphene devices, we measured an overall shift of ≈36 mV from 2×10^{-18} M to 2×10^{-6} M samples with shift of ≈6 mV even for the lowest ssDNA concentration of 2×10^{-18} TM compared to the negative control (PBS only). Due to the above differences in device performance, we focused on crumpled gFET sensors for the remaining experiments in our study.

Next, we investigated the physical adsorption of dsDNA on crumpled gFET biosensors by using a similar protocol as above and Figure 2d shows the electrical measurements. We added synthetic dsDNA (Table S1, Supporting Information) at concentrations from 2×10^{-18} M to 2×10^{-6} M and measured the Dirac point shifts for each condition as mentioned in the Materials and Methods section in Supporting Information. In contrast to the ssDNA experiments, the overall shift from 2×10^{-18} M to 2×10^{-6} M of dsDNA tested sequentially on the same device was only ≈6 mV, with shift for 2×10^{-6} M dsDNA itself being negligible. This confirms that dsDNA does not strongly adsorb on the crumpled gFET sensors and hence, we do not expect a significant contribution from dsDNA in our amplification experiments.

2.2. AFM Characterization of Physical Adsorption of Molecules on Graphene Surface

Structural features of the flat graphene surface with physiosorbed molecules were characterized using an AFM for different test cases and the results are shown in **Figure 3**. As seen in the AFM images in Figure 3a, the topography of a bare graphene surface is mostly flat (RMS roughness ≈0.6 nm) with

some defects. When physisorption of ssDNA molecules was tested by incubation for 15 min, followed by PBS and DI water rinsing, drying, and imaging in air, an increase in the surface roughness (RMS ≈1.5 nm) and morphology of the flat graphene was observed (Figure S5, Supporting Information). Since our platform differentiates amplified from non-amplified samples by detecting the reduction in primer concentrations and associated Dirac voltage shifts, we characterized graphene surfaces challenged with pre-amplification (time 0) and post-amplification (time 60) solutions diluted in PBS 1X. The solution dilution was the same as the ones used for electrical measurements in Figure 2. For all AFM physisorption tests, same protocol as above for ssDNA was used and more details are mentioned in the Materials and Methods section in Supporting Information. For pre-amplified test case shown in Figure 3b, an increase in the surface roughness and morphology of the flat graphene was observed similar to ssDNA tests, with RMS values of ≈1.5 nm, which was 2.4 times higher than the flat surface. The phase image confirms these features with the appearance of distinct black structures on the flat graphene surface. In contrast, when pre-amplified test case was tested for physisorption (Figure 3c), surface roughness of RMS≈0.45 nm was observed, which is similar to that of flat graphene. Phase image also shows smoother surface without black features. It must be taken into consideration that target dsDNA is in lower concentrations than ssDNA (primers) at time 0 of the amplification reaction. In the LAMP amplification reaction, primer consumption in forming replicates of target dsDNA causes the ssDNA concentration in the reaction to decrease. We can see in Figure 3c that high concentration of dsDNA (amplified product) as well as residual amplification molecules dried onto the graphene surface does not significantly change the graphene surface roughness. This was further confirmed in Figure 3d in which 100×10^{-9} M of synthetic dsDNA (sequence given in Table S1, Supporting Information) tested for physisorption on the graphene surface showed a similar roughness to that seen in Figure 3a,c. Note that we did not perform the adsorption studies on crumpled graphene as the AFM tip is not able to resolve differences with and without DNA adsorption on the crumpled graphene surface.

2.3. Attomolar *E. coli* DNA Detection using Crumpled gFET Biosensors

To test the ability of our crumpled gFET biosensor to distinguish positive amplification as compared to LAMP reactions where no target was present, we first performed real-time LAMP reactions for *E. coli* DNA with Evagreen dye to confirm that DNA amplification has occurred. **Figure 4**a,b shows the fluorescence measurements and threshold times for amplification of 4×10^{-18} M to 40×10^{-15} M *E. coli* genomic DNA using LAMP amplification reaction. For detection of *E. coli* DNA, primers (ssDNA) complementary to the eae gene was used to identify and begin the amplification reaction (see Table S1, Supporting Information, for sequences). Amplification of DNA concentrations from 40×10^{-15} M to 40×10^{-18} M can be seen for each replicate; however, only 1 out of 3 replicates for 4×10^{-18} M DNA concentration resulted in amplification. A 4×10^{-18} M translates to ≈2.4 copies μL^{-1} of starting sample and at these extremely
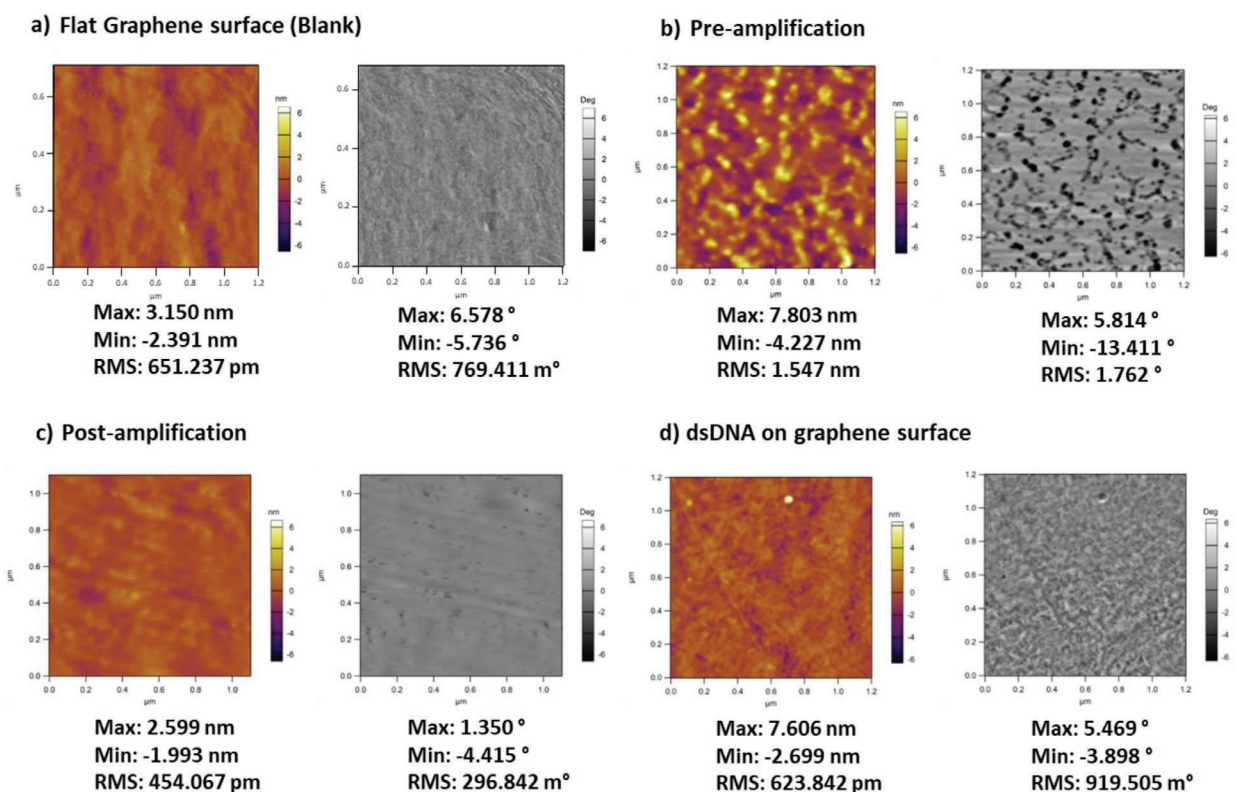
Figure 3. AFM images of flat graphene surface showing primer adsorption pre and post amplification. a) AFM image and phase image of bare graphene surface. b,c) AFM image and phase image of pre-amplified DNA (b) and post-amplified DNA (c) on flat graphene surface. The phase images show a rough surface with black structures indicating pre-amplification ssDNA (primers) adsorption to the graphene surface. Post-amplification, concentration of dsDNA is greater, which cannot be adsorbed on the graphene surface. Phase images show smoother surface with less black structures. d) AFM image and phase image of 1×10^{-6} M dsDNA on flat graphene surface, which show that dsDNA cannot be highly adsorbed on the graphene surface.

low concentrations, the sampling of the sample can result in errors. This thermocycler data will serve as a control for the following electrical measurements on these same samples post-amplification. These amplified and non-amplified samples (4×10^{-18} M, negative control) were diluted 1:100 in 1X PBS and sequentially tested on three separate crumpled gFET devices to measure the Dirac point shift for each case. The results are shown in Figure 4c. On each crumpled gFET sensor, we first measured the negative control sample before the beginning of the LAMP reaction (time = 0 min), after which the 40×10^{-15} M sample at time = 0 min was measured for the Dirac point shift. After 60 min of LAMP reaction, the samples were measured again starting with the negative control and each of the target DNA positive concentrations from 40×10^{-15} M to 4×10^{-18} M. Finally, we measured the negative control sample from time = 60 min again to confirm that the graphene surface was not saturated with DNA during the measurement. In Figure 4c, we can see that for each replicate the difference between amplified and non-amplified samples was greater than or equal to 4 mV showing the platform's ability to clearly distinguish the positive samples from the negative samples. The non-amplified 4×10^{-18} M samples served as blind tests and confirmed that our platform can distinguish these from the amplified 4×10^{-18} M samples. For amplified samples, we see lower Dirac point shifts compared to non-amplified samples, since the primers (ssDNA) are converted into dsDNA during the amplification and dsDNA

does not produce significant shift in Dirac point as shown previously in Figure 2d. The data from each replicate was then normalized to its lowest negative control Dirac voltage shift measurement and plotted in Figure 4d. All the normalized data was then clustered into "Amplified" and "Non-amplified" samples and a clear distinction between the two clusters can be seen in Figure 4e. This shows that negative samples can be clearly distinguished from positive samples with a detection limit of up to 4×10^{-18} M. Figures S1 and S2 (Supporting Information) show similar trends but with slightly lower average Dirac voltage shifts for 1X primer and 1:100 000 and 1:10 000 dilution in 1X PBS, respectively. Figure S3 (Supporting Information) shows the repeat of Figure 4 but with a reduced 0.1X primer concentration. Reduced primer concentration did not affect the electrical measurements but delayed the amplification threshold times by ≈20 min compared to 1X primer concentration, proving that a lower primer concentration results in delayed amplification and that are reactions are indeed primer concentration limited.

2.4. Zeptomolar *E. coli* DNA Detection using Crumpled gFET Biosensors

In **Figure 5**a, we show a schematic of a zeptomolar LAMP reaction in which ≈3 target *E. coli* dsDNA copies were spiked in 572 uL of water as the starting sample, resulting in an
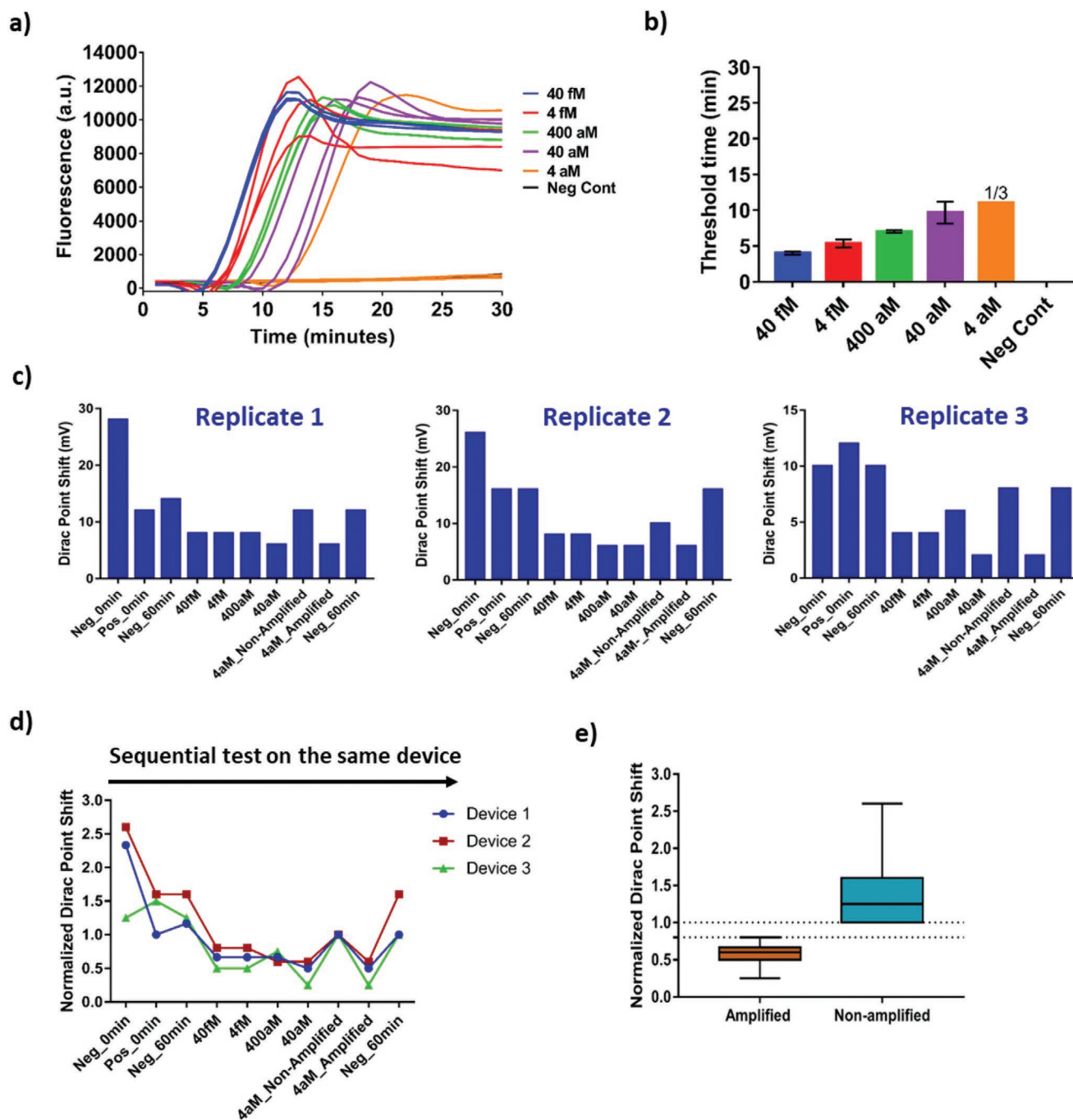
Figure 4. Attomolar *E. coli* DNA detection using crumpled gFET biosensors. a,b) Raw fluorescence data and amplification thresholds for different concentrations of *E. coli* DNA ($n = 3$). DNA concentrations from 4×10^{-18} M to 40×10^{-15} M were amplified over a 60 min LAMP reaction with 1X primer concentration per reaction (0.15×10^{-6} M of F3 and B3, 1.17×10^{-6} M FIP and BIP, and 0.59×10^{-6} M of LF and LB primers. Only 1 out 3 repeats for 4×10^{-18} M DNA concentration amplified. Both amplified and non-amplified DNA were measured for Dirac point shift. c) Absolute value Dirac point shifts for primer (negative control) and amplified dsDNA samples on three different FET devices. 1:100 dilution in 1X PBS of all post-reactions samples was made for Dirac voltage measurements. The shift for five amplified samples is lesser (8.4–10 mV) than that for five non-amplified samples (negative control and positive time zero samples). d) Normalized Dirac point shifts ($n = 3$) for each sample of the three devices in (c). e) Box and whisker plot for Normalized Dirac point shift for amplified (40×10^{-15} M–4×10^{-18} M) and non-amplified (negative and positive controls $t = 0$, negative $t = 60$, and unamplified 4×10^{-18} M) samples of the three devices in (c). The error bars show the range of the normalized data.

8×10^{-21} M concentration. LAMP reagents including the Bst polymerase were thereafter added for the reaction to occur at 65 °C for 60 min. Similarly, higher concentrations of *E. coli* dsDNA (40×10^{-21} and 400×10^{-21} M) were spiked and amplified in LAMP reactions. The products of each reaction were mixed and diluted 1:100 in 1X PBS and then electrically measured on
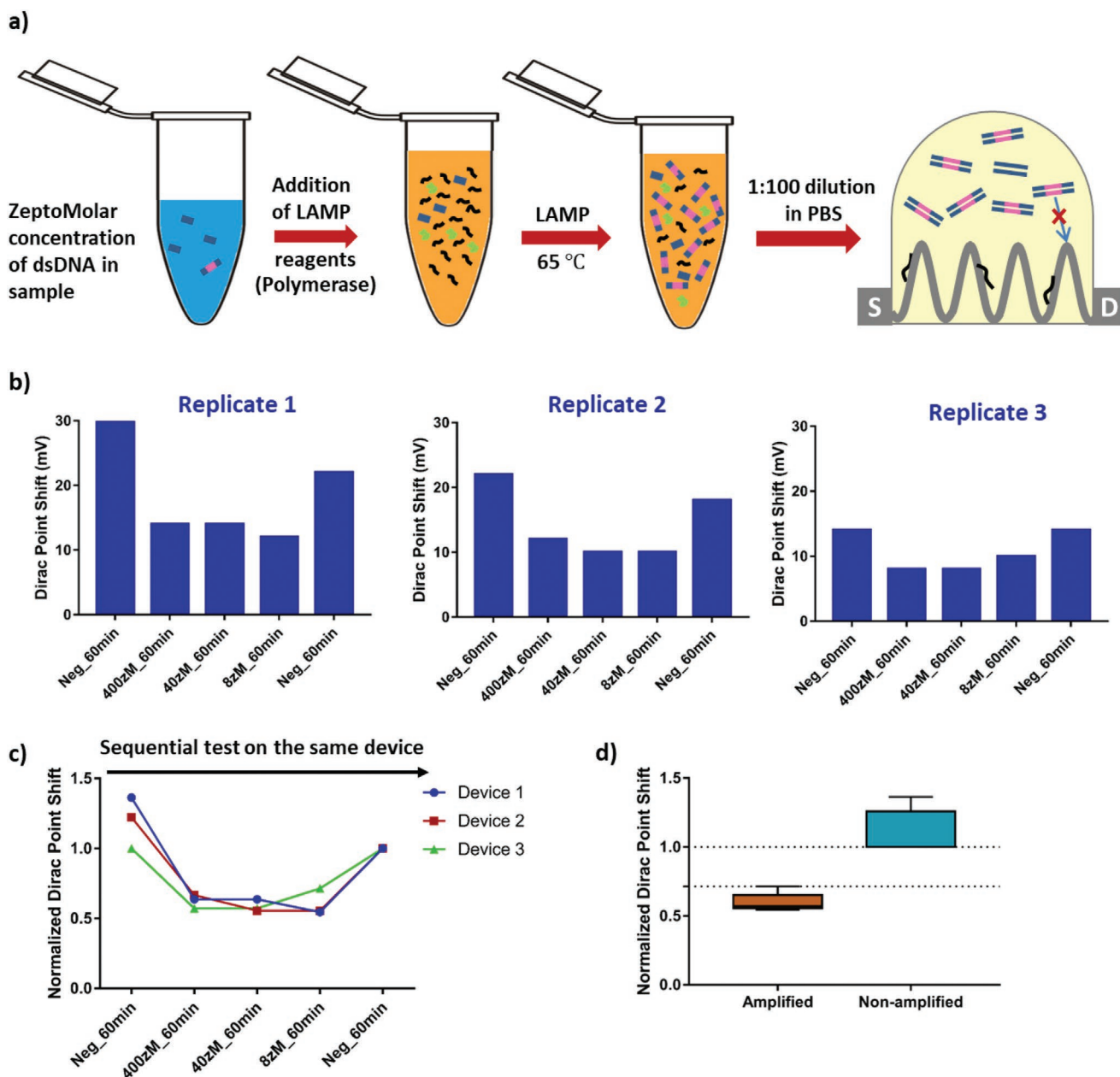
Figure 5. Electrical detection of amplified zeptomolar concentrations of DNA on crumpled gFET sensors. a) Process flow of zeptomolar LAMP reactions and detection on crumpled graphene. In 1 mL of diluted sample containing zeptomolar concentrations of target DNA, LAMP reagents such as primers and polymerase were added and the reaction was conducted at 65 °C. Amplified sample was loaded and incubated on crumpled graphene, after which Dirac point measurements were taken. b) Absolute value Dirac point shift for primer (negative control) and amplified dsDNA samples on three different FET devices. Starting DNA concentrations from 8×10^{-21} to 400×10^{-21} M were amplified over 60 min reaction with 1X primer concentration per reaction. Post reaction, 1:100 dilution in 1X PBS of all samples was made for Dirac voltage measurements. The shift for the three amplified samples is lesser (5.4–12.7 mV) than that for non-amplified samples (two measurements of negative control). c) Normalized Dirac point shifts ($n = 3$) for each sample of the three devices in (b). d) Box and whisker plot for the normalized Dirac point shift for amplified (40×10^{-15} M–4×10^{-18} M) and non-amplified (negative and positive controls $t = 0$, negative $t = 60$, and unamplified 4×10^{-18} M) samples of the three devices in (c). The error bars show the range of the normalized data.

the FET device. Sequentially testing on the same device, we first measured the negative control sample post-LAMP reaction (time = 60 min). Following that, we measured the 400×10^{-21}, 40×10^{-21}, and 8×10^{-21} M concentration sample reactions for Dirac point shift with PBS rinses in between. Finally, we measured the negative control sample again in order to confirm

that the graphene surface was not saturated with DNA during the measurement. In Figure 5b, three replicates of this experiment showed similar results. The negative control measurement showed a Dirac point shift of up to 30 mV. Differences in Dirac point shifts between replicates can be attributed to the variability in resistance of each device, which could be due to

ADVANCED
SCIENCE NEWS

www.advancedsciencenews.com

ADVANCED
FUNCTIONAL
MATERIALS

www.afm-journal.de

variability in the fabrication process. Nevertheless, the Dirac point shift for detection of amplification in all positive reactions (8×10^{-21} to 400×10^{-21} M) ranged from 8 to 14 mV. A difference of 4–18 mV was measured for Dirac shift between the 8×10^{-21} M sample and negative control in these three replicates. The data from each replicate was then normalized to its lowest negative control Dirac voltage shift measurement and plotted in Figure 5c. Figure 5d shows all the normalized data clustered into "Amplified" and "Non-amplified" samples and a clear distinction between the two clusters can be seen. This shows that negative samples can be clearly distinguished from positive samples with a detection limit of 8×10^{-21} M. Figure S4 (Supporting Information) shows the repeat of Figure 5 but with a reduced 0.1X primer concentration. Reduced primer concentration did not affect the electrical measurements, and amplified versus non-amplified samples could be distinguished clearly with no overlap.

3. Discussion

We demonstrate detection of enzymatic DNA amplification using crumpled gFET with detection limits down to zeptomolar target concentrations in the starting sample. Our platform deploys the evolutionary sensitivity and robustness of Bst polymerase combined with target specific primers, while using crumpled gFET to electrically detect the amplification by sensing the reduction in the primer molecules. We also characterize the physisorption of ssDNA, dsDNA, and LAMP reaction mix, pre- and post-amplification, to show lower physisorption of molecules (lower roughness in AFM) post-amplification due to reduced or consumed primers. Crumpled gFET provided better and higher sensitivity and Dirac voltage shifts in comparison to the flat counterpart and hence were chosen for our study. For our enzymatic reactions, we chose LAMP as it only needs a constant temperature for performing reactions and will allow easy translation into point-of-care and small footprint devices in the future. Moreover, since Bst polymerase has been applied to direct detection from complex matrices such as blood or saliva and requires specificity of six unique target specific primers, our platform will be more suitable for direct processing of complex samples in the future and will be superior to direct hybridization based approaches which rely on a single sequence/primer specificity. Compared to the conventional silicon-based ISFET approaches which sense changes in pH, require low buffer capacity reaction, and have a reported a detection limit of $>10 \times 10^{-18}$ M, our platform can sense target down to zeptomolar concentrations with electrical sensing possible directly in 1X PBS. Due to these reasons, we believe our platform will allow translation of complex lab-based diagnostic and genotyping amplification assays to truly point-of-care and bedside platforms in the future.

Supporting Information

Supporting Information is available from the Wiley Online Library or from the author.

Conflict of Interest

The authors declare no conflict of interest.

Author Contributions

A.G. and R.B. conceived the idea and designed the study. A.G., A.M. and V.F. performed the experiments. A.G., V.F., A.M., M.T.H and R.B. wrote the manuscript. All edited the manuscript.

[1] M. Sinha, J. Jupe, H. Mack, T. P. Coleman, S. M. Lawrence, S. I. Fraley, *Clin. Microbiol. Rev.* **2018**, *31*, e00089.
[2] N. Peker, N. Couto, B. Sinha, J. W. Rossen, *Clin. Microbiol. Infect.* **2018**, *24*, 944.
[3] A. Star, E. Tu, J. Niemann, J.-C. P. Gabriel, C. S. Joiner, C. Valcke, *Proc. Natl. Acad. Sci. U. S. A.* **2006**, *103*, 921.
[4] X. Dong, D. Fu, Y. Xu, J. Wei, Y. Shi, P. Chen, L.-J. Li, *J. Phys. Chem. C* **2008**, *112*, 9891.
[5] G.-J. Zhang, G. Zhang, J. H. Chua, R.-E. Chee, E. H. Wong, A. Agarwal, K. D. Buddharaju, N. Singh, Z. Gao, N. Balasubramanian, *Nano Lett.* **2008**, *8*, 1066.
[6] X. Dong, C. M. Lau, A. Lohani, S. G. Mhaisalkar, J. Kasim, Z. Shen, X. Ho, J. A. Rogers, L.-J. Li, *Adv. Mater.* **2008**, *20*, 2389.
[7] Y. Liu, S. Qin, Y. Song, Y. Feng, N. Lv, Y. Xue, F. Liu, S. Wang, B. Zhu, J. Ma, H. Yang, *Front. Microbiol.* **2019**, *10*, 598.
[8] M. Itahashi, *Arch. Ophthalmol.* **2010**, *128*, 535.
[9] G. Xu, J. Abbott, D. Ham, *IEEE Trans. Electron Devices* **2016**, *63*, 3249.
[10] C. Toumazou, L. M. Shepherd, S. C. Reed, G. I. Chen, A. Patel, D. M. Garner, C.-J. A. Wang, C.-P. Ou, K. Amin-Desai, P. Athanasiou, H. Bai, I. M. Q. Brizido, B. Caldwell, D. Coomber-Alford, P. Georgiou, K. S. Jordan, J. C. Joyce, M. La Mura, D. Morley, S. Sathyavruthan, S. Temelso, R. E. Thomas, L. Zhang, *Nat. Methods* **2013**, *10*, 641.
[11] C. Duarte-Guevara, V. V. Swaminathan, B. Reddy, J.-C. Huang, Y.-S. Liu, R. Bashir, *RSC Adv.* **2016**, *6*, 103872.
[12] R. Forsyth, A. Devadoss, O. J. Guy, *Diagnostics* **2017**, *7*, E45.
[13] P. A Rasheed, N. Sandhyarani, *Sens. Actuators, B* **2014**, *204*, 777.
[14] J. Ping, R. Vishnubhotla, A. Vrudhula, A. T. C. Johnson, *ACS Nano* **2016**, *10*, 8700.

[15] G. Xu, J. Abbott, L. Qin, K. Y. M. Yeung, Y. Song, H. Yoon, J. Kong, D. Ham, *Nat. Commun.* **2014**, *5*, https://www.nature.com/articles/ncomms5866.

[16] R. Hajian, S. Balderston, T. Tran, T. deBoer, J. Etienne, M. Sandhu, N. A. Wauford, J.-Y. Chung, J. Nokes, M. Athaiya, J. Paredes, R. Peytavi, B. Goldsmith, N. Murthy, I. M. Conboy, K. Aran, *Nat. Biomed. Eng.* **2019**, *3*, 427.

[17] M. T. Hwang, Z. Wang, J. Ping, D. K. Ban, Z. C. Shiah, L. Antonschmidt, J. Lee, Y. Liu, A. G. Karkisaval, A. T. C. Johnson, C. Fan, G. Glinsky, R. Lal, *Adv. Mater.* **2018**, *30*, 1802440.

[18] M. T. Hwang, P. B. Landon, J. Lee, D. Choi, A. H. Mo, G. Glinsky, R. Lal, *Proc. Natl. Acad. Sci. U. S. A.* **2016**, *113*, 7088.

[19] R. Campos, J. Borme, J. R. Guerreiro, G. Machado, M. F. Cerqueira, D. Y. Petrovykh, P. Alpuim, *ACS Sens.* **2019**, *4*, 286.

[20] C. I. L. Justino, A. R. Gomes, A. C. Freitas, A. C. Duarte, T. A. P. Rocha-Santos, *TrAC, Trends Anal. Chem.* **2017**, *91*, 53.

[21] Y. Liu, X. Dong, P. Chen, *Chem. Soc. Rev.* **2012**, *41*, 2283.

[22] W. Yang, K. R. Ratinac, S. P. Ringer, P. Thordarson, J. J. Gooding, F. Braet, *Angew. Chem., Int. Ed.* **2010**, *49*, 2114.

[23] A. K. Geim, K. S. Novoselov, *Nat. Mater.* **2007**, *6*, 183.

[24] S. Mao, J. Chang, G. Zhou, J. Chen, *Small* **2015**, *11*, 5336.

[25] S. Mao, G. Lu, J. Chen, *J. Mater. Chem. A* **2014**, *2*, 5573.

[26] S. Mao, *Graphene Bioelectronics*, Elsevier Inc., xxx **2018**, pp. 113–132. https://doi.org/10.1016/B978-0-12-813349-1.00005-6.

[27] B. Zhan, C. Li, J. Yang, G. Jenkins, W. Huang, X. Dong, *Small* **2014**, *10*, 4042.

[28] T.-Y. Chen, P. T. K. Loan, C.-L. Hsu, Y.-H. Lee, J. T.-W. Wang, K.-H. Wei, C.-T. Lin, L.-J. Li, *Biosens. Bioelectron.* **2013**, *41*, 103.

[29] B. Cai, S. Wang, L. Huang, Y. Ning, Z. Zhang, G.-J. Zhang, *ACS Nano* **2014**, *8*, 2632.

[30] C. Zheng, L. Huang, H. Zhang, Z. Sun, Z. Zhang, G.-J. Zhang, *ACS Appl. Mater. Interfaces* **2015**, *7*, 16953.

[31] K. Shoorideh, C. O. Chui, *Proc. Natl. Acad. Sci. U. S. A.* **2014**, *111*, 5111.

[32] M. C. Wang, S. Chun, R. S. Han, A. Ashraf, P. Kang, S. Nam, *Nano Lett.* **2015**, *15*, 1829.

[33] P. Kang, M. C. Wang, P. M. Knapp, S. Nam, *Adv. Mater.* **2016**, *28*, 4639.

[34] J. Leem, M. C. Wang, P. Kang, S. Nam, *Nano Lett.* **2015**, *15*, 7684.

[35] M. T. Hwang, M. Heiranian, Y. Kim, S. You, J. Leem, A. Taqieddin, V. Faramarzi, Y. Jing, I. Park, A. M. van der Zande, S. Nam, N. R. Aluru, R. Bashir, *Nat. Commun.* **2020**, *11*, 1543.

[36] M. Li, Y. Pan, X. Guo, Y. Liang, Y. Wu, Y. Wen, H. Yang, *J. Mater. Chem. A* **2015**, *3*, 10353.

[37] G. Wei, Q. Li, S. Steckbeck, L. C. Ciacchi, *Phys. Chem. Chem. Phys.* **2014**, *16*, 3995.

[38] S. Banerjee, J. Wilson, J. Shim, M. Shankla, E. A. Corbin, A. Aksimentiev, R. Bashir, *Adv. Funct. Mater.* **2015**, *25*, 936.

[39] P.-J. Huang, J. Liu, *Nanomaterials* **2013**, *3*, 221.

[40] L. Jansson, J. Hedman, *Biomol. Detect. Quantif.* **2019**, *17*, 100082.

[41] T. Notomi, *Nippon Rinsho. Jpn. J. Clin. Med.* **2007**, *65*, 957.

[42] A. Ganguli, A. Ornob, H. Yu, G. L. Damhorst, W. Chen, F. Sun, A. Bhuiya, B. T. Cunningham, R. Bashir, *Biomed. Microdevices.* **2017**, *19*, 73.

[43] T. Notomi, *Nucleic Acids Res.* **2000**, *28*, 63e.

[44] F. Wang, L. Jiang, B. Ge, *J. Clin. Microbiol.* **2012**, *50*, 91.